International Journal of Engineering & Technology, 8 (1.1) (2019) 44-52

International Journal of Engineering & Technology

Website: www.sciencepubco.com/index.php/IJET

Research paper

Chromium Carbonitride (CrCN) Coatings on SUS 316L with Potential Application as Bipolar Plate in PEMFC

Nur Fawwaz Asri[1], Teuku Husaini[2*], Abu Bakar Sulong[3], Edy Herianto Majlan[4], Wan Ramli Wan Daud[5], Bushroa Abdul Razak[6], Nabilah Afiqah Mohd Radzuan[7]

[1]*Institute of Fuel Cell, Universiti Kebangsaan Malaysia, 43600 UKM Bangi, Selangor, Malaysia.*
[2]*Department of Mechanical and Material Engineering, Faculty of Mechanical and Build Environment, Universiti Kebangsaan Malaysia*
[3]*Department of Chemical and Process Engineering, Faculty of Mechanical and Build Environment, Universiti Kebangsaan Malaysia*
[4]*Department of Mechanical Engineering, Faculty of Engineering, University of Malaya, 50603, Kuala Lumpur, Malaysia.*
[5]*Department of Chemical Engineering, Universitas Sumatera Utara, Medan, Indonesia*
**Corresponding author E-mail: t-husaini@ukm.edu.my*

Abstract

The effects of corrosion behavior and interfacial contact resistance (ICR) of sputtered chromium carbonitride (CrCN) on SUS 316L are investigated. The corrosion behavior of CrCN coatings as potential bipolar plates in proton exchange membrane fuel cells (PEMFCs) are studied by potentiodynamic tests in 0.5 M sulfuric acid (H_2SO_4) with a scan rate of 1 mV/S. The ICR values are measured to evaluate electrical conductivity. The surface topography and roughness are monitored by atomic force microscopy (AFM) to investigate the surface features of CrCN coatings that correspond to the X-ray powder diffraction (XRD) analysis. The diffraction peak of CrCN has a current density (I_{corr}) of 0.1 µA cm^{-2} and ICR of 2.12 mΩ cm^2 at 80 ºC after the coated 316L is polarized. The formed metal nitrides and carbides possess prominent physical and chemical properties, such as superconductivity, high hardness, high melting points, high electrical conductivity and good corrosion resistance. Favorable factors are observed in CrCN of Sample C with 150 W and 80 min deposition that resists corrosion either at the anode or cathode side in the PEMFC. Coating materials using CrCN are proposed to improved bipolar plates, to achieve the single cell performance in PEMFCs.

Keywords: *CrCN; SUS 316L; bipolar plate; corrosion behavior; interfacial contact resistance.*

1. Introduction

SUS 316L are promising materials as bipolar plates due to their many advantages, such as high electrical conductivity and mechanical strength, good machinability, and relatively low cost for mass production. Metal bipolar plate coating has been extensively investigated under acidic working conditions of PEMFCs [1, 2]. Metal bipolar plates at the anode side are prone to dissolution, and they decrease the electrical conductivity of fuel cells. Bipolar plates are one of the components of a fuel cell power system that use hydrogen energy and show good potential in ensuring a clean atmosphere and efficient transportation [3]. In fact, most industrial companies in Japan, Korea and Europe are already using hydrogen energy and power their vehicles without emitting harmful carbon dioxide responsible for global warming [4]. Thus, this approach delivers considerable energy for fuel and implies that a vehicle that uses hydrogen fuel will travel farther than a vehicle with the same amount of traditional petrol [5].

Strong materials with high electrical conductivity are produced by carbon coatings with a thickness of less than 1 µm in PEMFC operating conditions [6]. However, a passivation layer is easily formed at the cathode side and the ICR between the bipolar plate and the gas diffusion layer increases due to corrosion [7]. In ensuring a high corrosion protective layer at cathodic environments, chromium nitride (CrN) coatings should have high corrosion resistance due to their dense equiaxed crystallites after deposition [8]. Alternative coatings of chromium carbide (Cr-C) and chromium nitride and carbonitride (Cr-N-C) also improved electrical conductivity and corrosion resistance and considerably decrease current density (I_{corr}) and ICR values [9, 10]. These Cr coatings have been extensively investigated to improve their structure and toughness by using different compositions and techniques.

The surface modification criteria to formed CrCN coating as bipolar plates are required because the oxidation layer is easily formed due to the negative electrons release from water (H_2O) to air. On the basis of this characteristic, CrCN coatings were proposed in the current work as anticorrosion bipolar plates in PEMFC using PVD sputtering. In this work, SUS 316L plates were coated with CrCN using physical vapor deposition (PVD) sputtering to obtain a coating that conducts electrons and protects against corrosion. The ICR, corrosion and physical properties of SUS 316L plate materials were presented. On the basis of ICR and corrosion resistance measurements, the investigated SUS 316L plates with CrCN sputtering showed good potential as bipolar plates in PEMFCs.

2. Experimental Details

2.1. Substrate material

Stainless steel 316L samples containing 16.4 wt.% Cr, 10.1 wt.% Ni, and 1.9 wt.% Mo (balanced with Fe) were used in our experiments. The samples for sputtering were cut into a disk (coupon) with a diameter and thickness of 20 and 3 mm, respectively. Before sputtering, the samples were polished with silicon carbide abrasive paper with grit of 400–1200, followed by polishing with 6 and 1 micron diamond suspension. A small thickness enables lightweight materials to sustain their reasonable strength for bipolar plates [11]. The samples were ultrasonically cleaned in acetone for 30 min to remove any contaminants from the metal's surface before sputtering.

2.2. Plasma treatment

Sputtering was conducted in a TF450 PVD magnetron sputtering system (SG Co. Ltd., Singapore), equipped with commercially available Cr target measuring 3 and 101.6 mm in thickness and diameter. One target was fixed above the substrate holder and was set to rotate at 4 rpm to ensure uniform deposition. The parameters for the CrCN layer deposition on the SUS 316L plates were selected on the basis of the data collected from the literature review [1]. Therefore, Cr (purity 99.99 wt%) was used at the X target with supplied DC power, as shown in Fig. 1. The magnetron sputtering system used argon as the working gas mixed with reactive gas of nitrogen to improve the structures and properties of sputtered Cr [12]. The distance from the target to the substrates was approximately 100 mm. The shutter was closed and pre-sputtering was conducted for 5 min to clean and remove any contaminants from the target. The sputtering process in the PVD chamber started after vacuum pumping to 2.0×10^{-3} Pa.

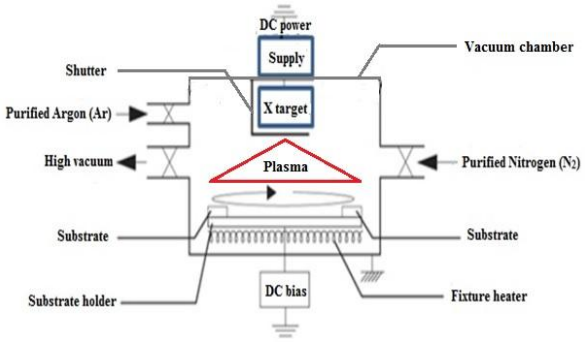

Fig. 1: Schematic assembly of the PVD system [13].

CrCN layer deposition was performed on the basis of the designated parameter and level for each experiment, as tabulated in Table 1. Three main parameters namely gas flowrate, DC powers, and deposition time, were investigated. 316L plates were initially coated with a CrCN layer under nitrogen and argon environment at a ratio of 1:5.

Table 1: Investigated deposition parameters and levels in the experiments.

Sample	Parameter			
	Gas flowrate (sccm)		DC power (W)	Deposition time (min)
	N_2	Ar		
A	8	40	50	40
B	8	40	100	60
C	8	40	150	80

2.3. Characterization method

Crystal orientations along the coating surface and crystallinity properties were examined by a BRUKER aXS-D8 Advance Cu Kα diffractometer at room temperature. The scanning angle (2θ) was varied from 20° to 80° with a step size of 0.02° and radiation wavelength, λ = 1.5408 A. The surface topography and roughness of the coated stainless steel samples at different parameters were measured by atomic force microscopy (AFM). The samples were half covered with masking tape to enable the thickness of any deposited coating for the step height profiles. For embrittlement prediction of austenitic stainless steel modification layer, Vickers microhardness tests were performed on the surfaces between SUS 316L and CrCN-coated. Applying 3 kg force with a dwell time of 15 s, five replicate tests were conducted. The density of the sample was measured using the standard Archimedes method using a balance with precision of 0.001 g.

2.4. Interfacial contact resistance (ICR)

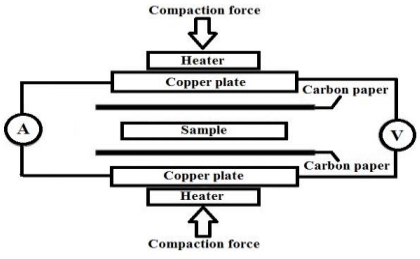

Fig. 2: Schematic of the test assembly for the ICR system.

The measurement values of ICR are determined by the voltage drop (R=VA/I) between the coated and uncoated samples of CrCN during the experiment. The surface ICR of the bipolar plate of CrCN was measured by placing the bipolar plate between the carbon paper (as GDL) under the real simulation condition and by measuring the voltage drop (R=VA/I) between the samples, whereas R is the electrical contact resistance, V is the voltage drop through the setup, I is the applied current and A is the surface area. The diameters of the piston and metal plates were 40 and 20 mm, respectively. The ICR was observed for the preferred parameter at the temperature of 40 °C to 80 °C. The applied current was 1 A. The compaction force applied during the experiment was 150 N cm^{-2} which was recorded by a Keithly meter device. Current (I) was sent in a complete setup and potential (V) was measured through a circuit in different preheating temperatures of 40 ºC, 60 ºC, and 80 ºC. Fig. 2 shows the schematic of the ICR based on the ICR setup [14, 15]. Voltage (V) and the total resistance across the test section before and after coating were measured [16, 17]. R1 refers to the resistance of two copper plates, and R2 referred to the resistance of GDL with CrCN-coated sample. Therefore, the ICR was equal to the total resistance in the test assembly, (R1 + R2 /2).

2.5. Electrochemical measurement

Electrochemical measurements were conducted on a radiometer analytical equipment by potentiostat PGZ100 (Voltalab 10). The procedure was controlled using the VoltaMaster 4 electrochemical software. A flat cell was used for the coupon substrate at room temperature in a solution of 0.5 M sulphuric acid (H_2SO_4). The SUS 316L substrate was used as the working electrode, a saturated calomel electrode Ag/AgCl (SCE) was used as reference electrode, and a platinum electrode acted as the counter electrode. All potentials were referred to the SCE during the experiment. The substrate was stabilized at open circuit (OCP) for 1 h and was polarized from OCP with a scan rate of 1 mV/s.

2.6. Cell Performance

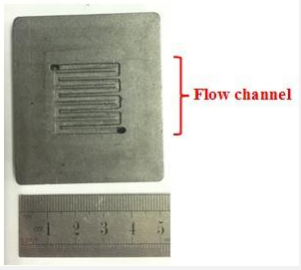

(a)

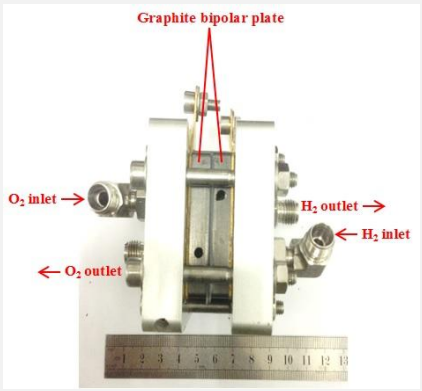

(b)

Fig. 3: Bipolar plates made from graphite (a) graphite bipolar plate with serpentine flow channel and (b) single cell bipolar plates.

Based on the graphite bipolar plates as references, a single cell stack were prepared using the CrCN-coated SUS 316L bipolar plates. Thickness of the CrCN-coated bipolar plates was 3 mm with serpentine flow field designed of 25 x 1.x 0.8 mm, as in Fig. 3(a). Five layered membrane electrode assembly (MEA) with active area 25 x 25 mm, integrated gas diffusion layers (GDL) were used. Pt loading was 0.5 mg/cm² and a membrane (Nafion® 212) was 0.002", with 410 um thick carbon cloths GDL. In providing anode and cathode gas in the fuel cell system, the bipolar plates separate individual cells of the fuel cell stack as in Figure 3(b). Hydrogen and oxygen gases went into the cell to react with the anode and cathode, respectively. Hydrogen gas continuously flows in the anode and produces H^+ ions. Only positively charged H^+ ions passed through the membrane, whereas negatively charged electrons flow to the electrical circuit to generate electrical power. Oxygen continuously flows in the cathode and then combined with H^+ ions. The negative electrons from water (H_2O) are released to the air. It can be seen that graphite bipolar plates is thicker and the weight volume increase. It is considered that the alternative materials to graphite are SUS 316L, which provided a good alternative to graphite bipolar plates. Since the bipolar plate requires fabrication of flow channels, SUS 316L with high ductility provides ease of manufacturing.

3. Result and Discussion

3.1. Characteristics of CrCN coatings

The result of the XRD analysis was used to evaluate the surface structure of a typical CrCN coating. XRD patterns for SUS 316L using Cr target electrodeposition are presented in Fig. 4 at different deposition times and supplied DC power. The peaks of Cr and Ni in SUS

316L plates were detected at 43.5º, 50.4º, 74.4º and 44.5º, which corresponded to the (110), (200), (200), and (111) crystal planes of the face centered cubic structure, respectively. CrCN peaks present in the substrates after coating corresponded to Sample A (130), Sample B (120) and Sample C (111). Few carbons were observed in the subsurface because carbon atoms can react with chromium atoms, to form a chromium carbide layer at the sample's surface and diffuse through this layer, thereby presenting a barrier for carbon diffusion [18]. In addition, nitrogen atoms are diffused through the chromium nitride layer. CrCN formations with varying ratios of Cr:C:N were observed on the samples surface and subsurface, respectively. However, CrNi was only observed in Sample B and Sample C at 50.4º and 74.4º, which corresponded to the (200) crystal plane. This layer acted as a barrier for nitrogen diffusion. Therefore, an insufficient nitrogen available in the subsurface region because nitrogen ions could not diffuse through the layer to form nitrides [9].

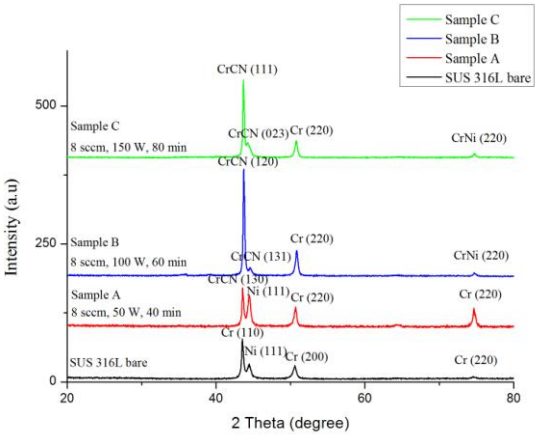

Fig. 4: XRD graph pattern for SUS 316L before and after coating with different CrCN coating parameters.

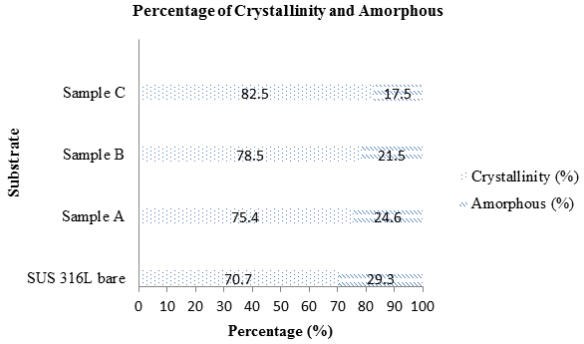

Fig. 5: Percentage of crystallinity and amorphousness of samples before and after CrCN coatings with different parameters.

As shown in Fig. 5, percentage of crystallinity and amorphousness were gained from the XRD analysis. The crystallinity (%) increased and amorphousness (%) decreased after coating. The highest crystallinity was 82.5 % and the lowest amorphousness was 17.5 % by Sample C with 150 W power and 80 min deposition. CrCN coating on SUS 316L substrates was performed well with rigid crystalline structure and low amorphousness to break the coating layer. A low percentage of amorphousness was beneficial for the long-term endurance of the CrCN coating in acidic PEMFCs with low corrosion rates. The CrCN coating layer performed well with nano roughness surfaces and high crystallinity in terms of preventing corrosion attack [19] without easily changing the phase formation and structure, without involving the bias voltage (increasing the sputtering yield) and substrate temperature [19, 20]. The result revealed that the argon-nitrogen gas mixture condition increased the hardness and strength of the layer due to nitrogen dissolution and surface roughness reduction of the CrCN coating [20].

3.2. Through plane ICR

The ICR with the current of 1 A for each sample was observed as shown in Table 2. The ICR was measured at temperatures of 40 ºC, 60 ºC, and 80 ºC. SUS 316L plates without CrCN coating were obtained at high temperature with low ICR values. By contrast, the ICR values decreased further for the SUS316L coated with CrCN at different level parameters for Sample A, Sample B, and Sample C.

Table 2: The ICR and potential (V) for SUS 316L with different coating parameter at 1 A.

Material	Sus 316L bare		Sample A		Sample B		Sample C	
T (ºC)	V (V)	ICR (mΩ cm²)	V (V)	ICR (mΩ cm²)	V (V)	ICR (mΩ cm²)	V (V)	ICR (mΩ cm²)
40	2.94	4.63	0.64	3.61	0.97	3.09	1.33	2.52
60	2.29	3.60	0.19	3.29	0.71	2.49	0.88	2.21

80	1.89	2.97	0.19	2.67	0.39	2.34	0.54	2.12

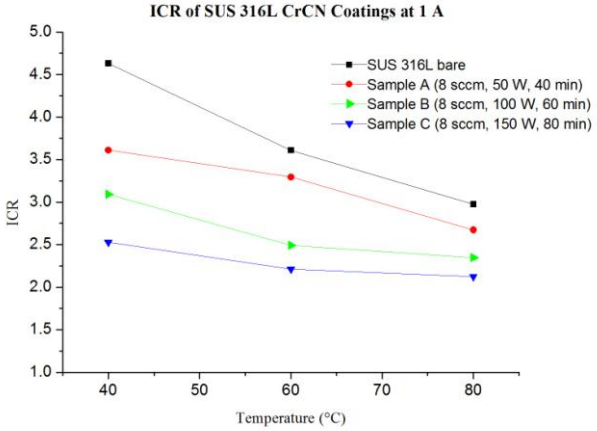

Fig. 6: ICR pattern for SUS 316L with different coating parameters at 1 A.

The graph pattern in Fig. 6 indicates the ICR values of SUS 316L plates versus temperature. Overall, the ICR values decreased with the increase of temperature from 40 °C to 80 °C. Sample C had a lower ICR value compared with the other samples, and most of the samples presented the same general behaviour as that of Sample C but with slightly higher ICR values. The exception was the bare 316L, which was higher than the other samples but still below the DOE requirement. The ICR results showed the performance of the samples in order of Sample C > Sample B > Sample A > bare 316L. Sample C with CrCN-coated remained an excellent candidate as metal bipolar plate for PEMFCs since the small differences in ICR values.

The difference and similarity percentages of the ICR between the uncoated bare 316L and Sample C were 59 % and decreased to 33 % after coating. Improvements with the small similarities were observed after CrCN coatings. The influence of low temperature on austenitic stainless steels that contained high Cr and Ni reduced the ICR with the increase of temperature [21]. Overall, Sample C obtained the lowest ICR values after Cr coating. The ICR values for SUS 316L plates after CrCN coating were between 2.52 mΩ cm² to 2.12 mΩ cm², thereby meeting the requirement of U.S DOE.

3.3. Electrochemical polarization and stability

Potentiodynamic polarization tests were conducted to evaluate the corrosion behaviour of uncoated SUS 316L and CrCN-coated samples. The polarization curves are shown in Fig. 7. For all samples, passive and trans-passive regions appeared in the graph pattern of the polarization curves. The aeration and presence of acidic and warm solution provided an aggressive medium for the samples. Thus, a passive layer was readily formed on the surface of the samples. The increase of corrosion current density in the anodic branch was slower for the CrCN-coated than for the uncoated SUS 316L. Corrosion occurred due to the increase of current densities.

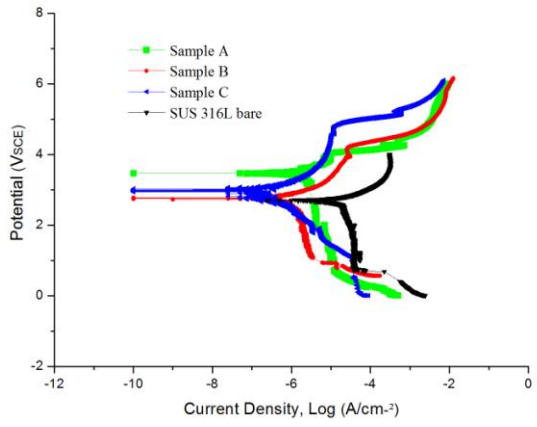

Fig. 7: Polarization curves for uncoated SUS 316L and CrCN-coated SUS 316L in 0.5 M H_2SO_4.

Table 3: Electrochemical parameter properties of uncoated SUS 316L and CrCN-coated SUS 316L.

Plate	E_{corr} (V)	I_{corr} (μA cm^{-2})	Tafel Slopes (mV)		CR (μm/year)
			$ß_a$	$ß_c$	
SUS 316L	2.7	4.9	147.6	– 185.7	207.7
Sample A	3.5	0.5	125.6	– 175.2	19.2

Sample B	2.7	0.2	369.1	– 684.7	8.1
Sample C	2.6	0.1	45.7	– 47.8	5.8

Additional information on the potentiodynamic polarization results are shown in Table 3. The corrosion current density and corrosion potential amounts were calculated from the intercept of the Tafel slopes. The uncoated SUS 316L showed higher corrosion densities and corrosion potentials than CrCN-coated samples. CrCN coatings efficiently protected the SUS 316L substrates [22]. According to Fig. 7, the initial OCP values for Sample A, Sample B, Sample C and SUS 316L bare were 3.3 V, 3.8 V, 4.1 V, and 2.6 V (Ag/AgCl) in H_2SO_4 solution. This value turned into a passive state after less than 3600 s. SUS 316L bare was in passive state under test condition from 0.8 to 1.5 V, with corrosion current density (I_{corr}) at 2.7 V (SCE) as the operating condition. The CrCN-coated SUS 316L in the potential range of 2.7 to 3.5 V (SCE) at room temperature have similar general features. The highest E_{corr} was 3.5 V which is produced by Sample A.
It can be observed that by increasing the E_{corr} value, the I_{corr} value will decrease and potentially reduce the corrosion attack at 0.5 µA cm^{-2}. In comparison, Sample B exhibited much better corrosion resistance and the I_{corr} recorded was 0.2 µA cm^{-2} at 2.7 V, respectively. However, the lowest I_{corr} 0.1 µA cm^{-2} was recorded by Sample C and the passivation helps to delay the corrosion process before transpassivation behaviour rapidly increase to the anodic region. The potential 0.6 V (SCE) is the operating potential of the cathode side in a PEMFC. Several researchers, such as Yi et al., assumed that the corrosion current density of bipolar plates in simulated cathodic condition should be less than 1 µA cm^{-2} at 0.6 V (SCE) in potentiodynamic polarization test [9]. No agreement is established in using the corrosion current density at 0.6 V (SCE) to predict bipolar plate corrosion in operating cathode condition. CrCN coatings efficiently protected the SUS 316L substrates [22]. In addition, PVD coatings are proven to be valuable to resist corrosion [23]. All samples of CrCN-coated SUS 316L had I_{corr} less than 1 µA cm^{-2}. Sample C was recorded as the best parameter because more cathodic region of passivation and lowest I_{corr} (0.1 µA cm^{-2}), which satisfies the DOE criterion.

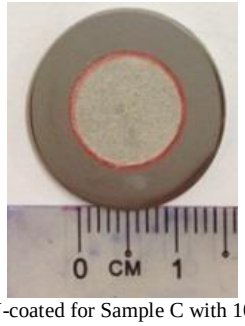

Fig. 8: Macrostructure observation of CrCN-coated for Sample C with 10 mm surface area exposed in 0.5 M H_2SO_4.

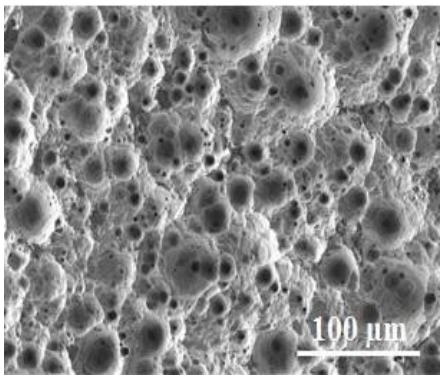

Fig. 9: Polarization curves for CrCN-coated for Sample C in 0.5 M H_2SO_4.

SEM surface morphology analysis results of CrCN-coated for Sample C after polarization test are shown in Fig. 8. The solid surface of Sample C was activated by immersion in H_2SO_4 solution and small sized pore was created, as shown in Fig. 9. These pores contained a mixture of air, (but depleted to some extent of oxygen), arising from the H_2SO_4 solution [24]. Upon immersion, deep pores were created on the oxide layer through the grain structure. It created small pits which did not propagate into large ones. The immersed area had a loss of weight from 0.0074 g/cm^3 to 0.059 g/cm^3 due to the localized attack as in Fig.9.

3.4. AFM characteristics of CrCN

The surface topography and roughness of the coated stainless steel samples at different parameters for Sample A, B and C were examined using AFM, and the results are shown in Fig. 10. The AFM images show the detailed surface feature of the half-covered CrCN coatings on the SUS 316L plates. The overall ridges were created by polishing the coupon plates rather than covering them with masking tape during step height thickness preparation. As shown in Fig. 10, granular shaped grains grew on the coated surfaces. The size and height of the ridges decreased with the increase of DC power and deposition time. Sample A for CrCN-coated SUS 316L with 50 W and 40 min deposition had more ridges than those shown in Sample B (100 W and 60 min) and Sample C (150 W and 80 min). Furthermore, increased DC power also exhibited fewer ridges and thicker CrCN layer. Obviously, the AFM results show that surface roughness significantly increases with the increase of DC power and deposition time possibly because of the high Cr grain growth at high current densities. In addition, the coatings were transformed from crystalline state to amorphous state, and the grain size gradually became small [18].

Roughness (R_a)	AFM images
Sample A 17.85 nm	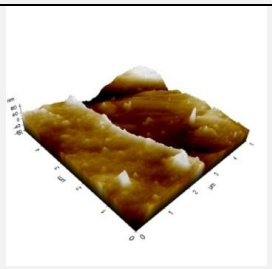
Sample B 202.79 nm	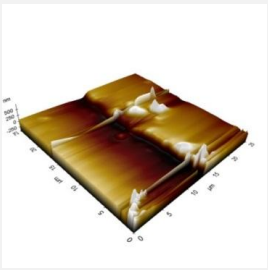
Sample C 242.26 nm	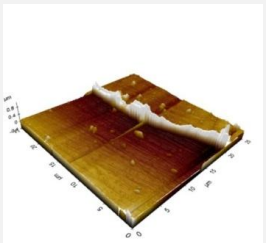

Fig. 10: AFM images of SUS 316L substrates that were half-covered to enable the thickness after coating: Sample A, Sample B and Sample C.

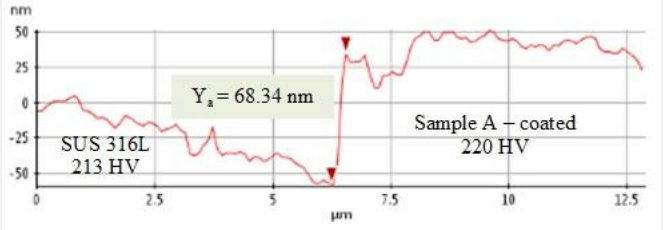

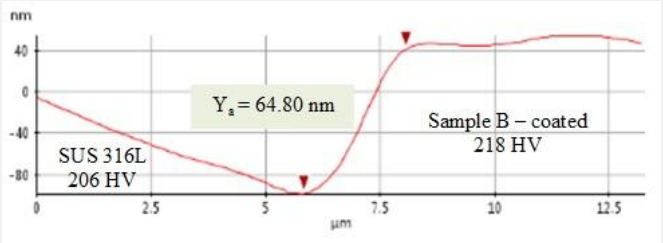

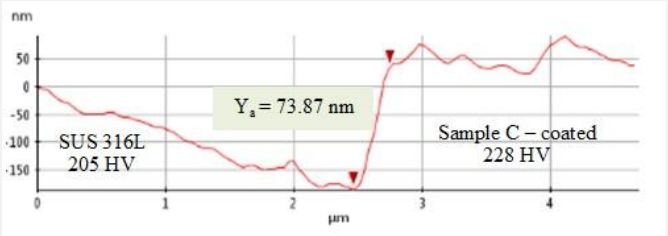

Fig. 11: Graph of step height versus distance between CrCN-coated and SUS 316L plates.

The CrCN-coated SUS 316L were rough with the increase of deposition time and current densities; this outcome is in agreement with the XRD observations. In comparison with Sample A and B, Sample C obtained the highest surface roughness at 242.26 nm with 73.87 nm of CrCN thickness profile. The CrCN thickness step height (Y_a) profiles were measured from the AFM. The step height profiles were summarized in Fig. 11. Micro-hardness test was intended at five regions of the surface between CrCN-coated and uncoated SUS 316L.

The uncoated SUS 316L average values were 205 HV to 213 HV, and increased after coatings. The highest hardness average value was recorded by Sample C at 228 HV, while 220 and 218 HV were recorded for Sample A and B.

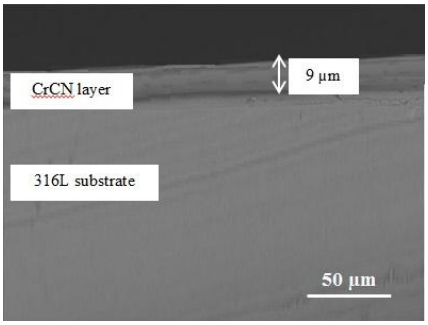

Fig. 12: Cross-section of SEM micrograph image of CrCN-coated SUS 316L for Sample C.

Gas flowrate of 8 sccm (standard cubic centimeters per minute) and DC power of 150 W (watt), with 80 min (minutes) deposition represents by Sample C gives good response for corrosion resistance and ICR. On top of good mechanical properties, the CrCN coatings thickness was 9 µm. The cross-sectional SEM micrograph of CrCN-coated SUS 316L is shown in Fig. 12. Pores were observed through the entire coating at 50 µm magnification. A shadowing effect of irregular surfaces was clearly observed between the two layers due to the low substrate temperature deposition. The coating growth controlled by surface diffusion corresponded to a coating structure with low kinetic energy for Sample C [25].

3.5. CrCN coatings on the cell performance of PEMFC

Single cells were tested using SUS 316L and CrCN-coated SUS 316L to evaluate performance of the bipolar plates. The single cells were operated 2 h for activation, before the measured reading. Fig. 13 shows initial performance of the single cells. From the performance curve, CrCN-coated performance increase than SUS 316L. The corrosion during activation process also reduced due to high contact resistance [26]. At the cell voltage of 0.6 V, the single cells employed by SUS 316L and CrCN-coated bipolar plates produced current density of 110 and 150 mA/cm^2, respectively. In this study, the current density before coating was lower compared to CrCN-coated. This is due to the lifetime for CrCN-coated was prolonged to 430 mA/cm^2, and the performance reduced slowly and steadily operates. However, the maximum power density exhibit by SUS 316L and CrCN-coated were 104 and 117 mW/cm^2 at 0.44 V. The challenges are to improve the initial performance with good operating condition above 0.6 V as a function of operating time [27] The performance pattern for CrCN-coated and SUS 316L before coating increased 11 %. Though, the activation process could reduce the cell performance of SUS 316L before and after CrCN coatings.

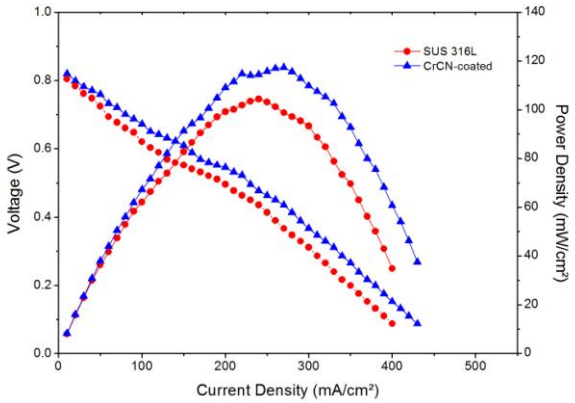

Fig. 13: *i–V* curves for the single cell stack; active electrode area = 5 cm^2, T_{cell} = RT, $\lambda H_2 = 0.5$, $\lambda O_2 = 5$, and P = 1 atm.

4. Conclusion

SUS 316L samples were sputtered and formed CrCN-coated for 40, 60, and 80 min to determine the improvement in corrosion current density and ICR. The CrCN layer with a thickness of 9 µm was formed on the surface region of Sample C with high peaks at the (111) crystal plane. The potentiostatic tests showed the good performance of corrosion resistance <1 µA cm^{-2} of the CrCN-coated SUS 316L as compared with its condition before coating. Existing holes from corrosion were present, but few oxidations occurred after CrCN coatings. The ICR achieved the DOE target of below 10 mΩ cm^2. The ICR values of SUS 316L plates decreased with the increase of temperature. However, the ICR of austenitic SUS 316L responded towards temperature. The ICR value of 2.12 mΩ cm² at 80 ºC showed that I_{corr} of Sample C with 150 W and 80 min deposition had a low current density of 0.1 µA cm^{-2}, thus displacing E_{corr} toward 2.7 V. This outcome caused considerable passivation to obtain good corrosion resistance. The XRD pattern showed that the used DC power and deposition time influenced the density and homogeneity of the coating. The appropriate DC power with the increase of substrate temperature during sputtering reduced the ICR within the DOE target. By contrast, CrCN elements after coating aided in improving the mechanical properties and corrosion resistance of SUS 316L to serve as bipolar plates, mainly at cathode in PEMFCs. The effect of life time test of single cell CrCN-coated SUS 316L bipolar plate and operating condition above 0.6 V at a constant current density will be included in the future studies.

Acknowledgement

The authors gratefully acknowledged everyone that provided valuable suggestions and collaboration in this research, including the Fuel Cell Institute UKM, Ministry of Higher Education, and FRGS/1/2017/TK10/UKM/02/6 Grants for sponsoring the research studies. We also extend our gratitude to the Faculty of Engineering, University Malaya for the significant support in the research on metal bipolar plates coating.

References

[1] N.F. Asri, T. Husaini, A.B. Sulong, E.H. Majlan, W.R.W. Daud (2017), Coating of stainless steel and titanium bipolar plates for anticorrosion in PEMFC: A review, International Journal of Hydrogen Energy, 42, 9135-9148.
[2] R. Taherian (2014), A review of composite and metallic bipolar plates in proton exchange membrane fuel cell: Materials, fabrication, and material selection, Journal of Power Sources, 265, 370-390.
[3] J.-J. Hwang (2013), Sustainability study of hydrogen pathways for fuel cell vehicle applications, Renewable and Sustainable Energy Reviews, 19, 220-229.
[4] A.F. Ambrose, A.Q. Al-Amin, R. Rasiah, R. Saidur, N. Amin (2017), Prospects for introducing hydrogen fuel cell vehicles in Malaysia, International Journal of Hydrogen Energy, 42, 9125-9134.
[5] R.A. Huggins (2016), Hydrogen Storage, Energy Storage, Springer, pp. 95-118.
[6] T. Fukutsuka, T. Yamaguchi, S.-I. Miyano, Y. Matsuo, Y. Sugie, Z. Ogumi (2007), Carbon-coated stainless steel as PEFC bipolar plate material, Journal of Power Sources, 174, 199-205.
[7] W. Mingge, L. Congda, H. Tao, C. Guohai, W. Donghui (2016), Chromium interlayer amorphous carbon film for 304 stainless steel bipolar plate of proton exchange membrane fuel cell, Surface and Coatings Technology, 307, 374-381.
[8] C. Liu, Q. Bi, A. Leyland, A. Matthews (2003), An electrochemical impedance spectroscopy study of the corrosion behaviour of PVD coated steels in 0.5 N NaCl aqueous solution: Part II.: EIS interpretation of corrosion behaviour, Corrosion Science, 45, 1257-1273.
[9] P. Yi, L. Peng, T. Zhou, H. Wu, X. Lai (2013), Cr–N–C multilayer film on 316L stainless steel as bipolar plates for proton exchange membrane fuel cells using closed field unbalanced magnetron sputter ion plating, international journal of hydrogen energy, 38, 1535-1543.
[10] Y. Zhao, L. Wei, P. Yi, L. Peng (2016), Influence of Cr-C film composition on electrical and corrosion properties of 316L stainless steel as bipolar plates for PEMFCs, International Journal of Hydrogen Energy, 41, 1142-1150.
[11] X.Z. Yuan, H. Wang, J. Zhang, D.P. Wilkinson (2005), Bipolar plates for PEM fuel cells-from materials to processing, Journal of New Materials for Electrochemical Systems, 8, 257.
[12] F. Alresheedi, J. Krzanowski (2017), Structure and morphology of stainless steel coatings sputter-deposited in a nitrogen/argon atmosphere, Surface and Coatings Technology, 314, 105-112.
[13] A. Bushroa, H. Masjuki, M. Muhamad (2011), Parameter optimization of sputtered Ti interlayer using Taguchi method, International Journal of Mechanical and Materials Engineering, 6, 140-146.
[14] [14] H. Husby (2013), Carbon Based Coatings for Metallic Bipolar Plates in PEM Fuel Cells, NTNU, Norwegian University of Science and Technology, pp. 1-106.
[15] S. Lee, N. Kakati, J. Maiti, S. Jee, D. Kalita, Y. Yoon (2013), Corrosion and electrical properties of CrN-and TiN-coated 316L stainless steel used as bipolar plates for polymer electrolyte membrane fuel cells, Thin Solid Films, 529, 374-379.
[16] Y. Hung, H. Tawfik, K. El-Khatib, H. El-Abd (2008), Corrosion and contact resistance measurements of different bipolar plate material for Polymer Electrolyte Membrane Fuel Cells, International Journal of Alternative Propulsion, 2, 72-85.
[17] S. Lædre (2011), Investigation of metallic bipolar plates for PEM fuel cells, Institutt for materialteknologi.
[18] H. Pengfei, J. Bailing (2011), Study on tribological property of CrCN coating based on magnetron sputtering plating technique, Vacuum, 85, 994-998.
[19] M. Kazmanli, M. Ürgen, A. Cakir (2003), Effect of nitrogen pressure, bias voltage and substrate temperature on the phase structure of Mo–N coatings produced by cathodic arc PVD, Surface and Coatings Technology, 167, 77-82.
[20] C.-H. Hsu, W.-C. Huang, Y.-P. Lee, W.-Y. Ho (2017), Effect of nitrogen atmosphere heat treatment on structure and wear behavior of CrAlSiN nanocomposite film, Surface and Coatings Technology, 320, 230-234.
[21] K. Lin, X. Li, Y. Sun, X. Luo, H. Dong (2014), Active screen plasma nitriding of 316 stainless steel for the application of bipolar plates in proton exchange membrane fuel cells, International Journal of Hydrogen Energy, 39, 21470-21479.
[22] Y. Kong, X. Tian, C. Gong, P.K. Chu (2018), Enhancement of toughness and wear resistance by CrN/CrCN multilayered coatings for wood processing, Surface and Coatings Technology, 344, 204-213.
[23] H.-P. Feng, C.-H. Hsu, J.-K. Lu, Y.-H. Shy (2003), Effects of PVD sputtered coatings on the corrosion resistance of AISI 304 stainless steel, Materials Science and Engineering: A, 347, 123-129.
[24] W. Griffiths, A. Gerrard, Y. Yue (2016), Oxide film defects in Al alloys and the formation of hydrogen-related porosity, IOP Conference Series: Materials Science and Engineering, IOP Publishing, pp. 1-6.
[25] M. Fenker, M. Balzer, H. Kappl (2014), Corrosion protection with hard coatings on steel: Past approaches and current research efforts, Surface and Coatings Technology, 257, 182-205.
[26] E. Cho, U.-S. Jeon, S.-A. Hong, I.-H. Oh, S.-G. Kang (2005), Performance of a 1kW-class PEMFC stack using TiN-coated 316 stainless steel bipolar plates, Journal of power sources, 142, 177-183.
[27] S. Shimpalee, V. Lilavivat, H. McCrabb, Y. Khunatorn, H.-K. Lee, W.-K. Lee, J. Weidner (2016), Investigation of bipolar plate materials for proton exchange membrane fuel cells, International Journal of Hydrogen Energy, 41(31), pp. 13688-13696.